Mechanical Systems and Signal Processing ▮ (▮▮▮▮) ▮▮▮–▮▮▮

Contents lists available at ScienceDirect

Mechanical Systems and Signal Processing

journal homepage: www.elsevier.com/locate/jnlabr/ymssp

Sensorless speed detection of squirrel-cage induction machines using stator neutral point voltage harmonics

Goran Petrovic, Tomislav Kilic *, Bozo Terzic

Faculty of Electrical Engineering, Mechanical Engineering and Naval Architecture, University of Split, 21000 Split, Croatia

ARTICLE INFO

Article history:
Received 27 July 2007
Received in revised form
29 May 2008
Accepted 15 June 2008

Keywords:
Induction squirrel-cage machines
Rotor slot harmonics
Sensorless speed detection

ABSTRACT

In this paper a sensorless speed detection method of induction squirrel-cage machines is presented. This method is based on frequency determination of the stator neutral point voltage primary slot harmonic, which is dependent on rotor speed. In order to prove method in steady state and dynamic conditions the simulation and experimental study was carried out. For theoretical investigation the mathematical model of squirrel cage induction machines, which takes into consideration actual geometry and windings layout, is used. Speed-related harmonics that arise from rotor slotting are analyzed using digital signal processing and DFT algorithm with Hanning window. The performance of the method is demonstrated over a wide range of load conditions.

1. Introduction

Estimators, observers, and spectral analysis methods are the frequently used techniques for sensorless speed estimation [1]. Sensorless speed estimation can provide robust, field-oriented torque control of an induction machine without a tachometer [2]. Most sensorless control schemes rely on estimation of the back EMF from stator voltages and currents, but the performance of speed estimators depends on the accuracy of the machine model and parameter estimator. Observers for speed estimation have a relatively long delay time that can limit speed detection during a transient.

In order to improve the robustness of sensorless speed estimation, parameter-independent magnetic saliency harmonics can be used to generate an accurate rotor speed signal, which can then be used to tune the parameters of a back-EMF-based observer. Saliency harmonics, which arise from rotor slotting and eccentricity, provide robust speed estimation because they are independent of time-varying motor parameters [3]. Digital signal-processing techniques can effectively extract saliency harmonics from the stator current, but they often require complex filtering techniques. Moreover, prior to digital sampling, an analog notch filter must be applied to reduce the spectral component of the fundamental frequency [2,8].

In this paper, a new method of determining rotor speed from the neutral point voltage of the induction machine is presented. The stator winding must be star connected and must have the neutral point accessible. Voltage is measured between the neutral of the machine and virtual null point realized by means of ideally balanced three resistors. In such way fundamental power supply harmonic is eliminated from measuring voltage signal and the strongest harmonic in that signal is the rotor slot harmonic. As the neutral point voltage has a value of only about 1 V, the voltage transducer is not necessary. Applying digital signal-processing techniques to neutral point voltage signal the frequency of speed-related harmonic is

* Corresponding author. Tel.: +385 21 305772.
E-mail addresses: goran.petrovic@fesb.hr (G. Petrovic), tkilic@fesb.hr (T. Kilic), bozo.terzic@fesb.hr (B. Terzic).

0888-3270/$ - see front matter © 2008 Elsevier Ltd. All rights reserved.
doi:10.1016/j.ymssp.2008.06.005

calculated. The proposed method has been demonstrated to work reliably for most standard induction squirrel-cage machines over a full range of load conditions.

2. Mathematical model of machine

A mathematical model of squirrel-cage induction machines with wye-connected stator windings was derived as theoretical background for speed detection using neutral point voltage signal [5–7]. In this model the saturation effects were negligible and uniform air-gap was assumed. Although stator neutral point voltage could be obtained as a sum of three phase voltages in the stator windings' equivalent circuits without a neutral line, in the derived model the neutral point voltage is calculated as voltage drop on the equivalent big resistor, which is set in a neutral line. Neutral point voltage calculation was chosen by reason of numerical stability problems in a simulation procedure. Schematic representation of the stator windings is shown in Fig. 1 where $\ell_{\sigma sg}$ is the leakage inductance, ℓ_{asas}, ℓ_{bsbs}, ℓ_{cscs} are magnetizing inductances of stator windings and ℓ_{asbs}, ℓ_{bscs}, ℓ_{csas} are mutual inductances.

The voltage equation for stator phase *as* can be written as

$$u_{as} - u_z = R_s i_{as} + \frac{d\psi_{as}}{dt} \tag{1}$$

where u_{as} is the stator voltage of phase *as*, u_z is the stator neutral point voltage, i_{as} is the current in phase *as*, R_s is phase resistance and ψ_{as} is the flux linkages of phase *as*. The stator voltage equation in the matrix form can be written as

$$\boldsymbol{u}_s = \boldsymbol{R}_s \boldsymbol{i}_s + \frac{d\psi_s}{dt}, \quad \boldsymbol{\Psi}_s = \boldsymbol{L}_s \boldsymbol{i}_s + \boldsymbol{L}_{sr} \boldsymbol{i}_r \tag{2}$$

where $\boldsymbol{u}_s = [(u_{as}-u_z)\ (u_{bs}-u_z)\ (u_{cs}-u_z)]^T$, $\boldsymbol{i}_s = [i_{as}\ i_{bs}\ i_{cs}]^T$, $\boldsymbol{\Psi}_s = [\psi_{as}\ \psi_{bs}\ \psi_{cs}]^T$, $\boldsymbol{R}_s = diag[R_s\ R_s\ R_s]$, $\boldsymbol{i}_r$ is the subvector of rotor current, $\boldsymbol{L}_{sr}$ is the submatrix of mutual inductance, and $\boldsymbol{L}_s$ is the submatrix of stator inductance.

In general, a mutual inductance function of two windings can be described by means of coil function $z(\gamma_s)$, which describes stator winding along the stator inner surface [7]. The approach based on the winding functions makes no assumption as to the necessity for sinusoidal MMF and therefore include all the space harmonics in the machine. The coil functions of stator phases for the analyzed machine are shown in Fig. 2.

A function of mutual inductance stator windings *as* and *bs* is given by

$$\ell_{asbs} = \frac{\mu_0}{\delta} \frac{d}{2} l_e \int_0^{2\pi} z_{as}(\gamma_s)\, z_{bs}(\gamma_s)\, d(\gamma_s) \tag{3}$$

where μ_0 is the permeability constant, d the average air-gap radius, l_e the length of stator stack, and δ the equivalent air-gap.

The rotor cage can be viewed as Q_r identical and equally spaced rotor bar. For that case, there are $2Q_r$ nodes and $3Q_r$ branches. Therefore, the current distribution can be specified in terms of Q_r+1 independent rotor currents. These currents comprise the Q_r rotor loop currents (i_μ), plus a circulating current in one of the end rings (i_{er}) [7].

Fig. 3 shows the schematic representation of the rotor cage where $\mu = 1, 2, \ldots, Q_r$ is the loop number, r_{rb} the rotor bar resistance, r_{er} the rotor end ring segment resistance, $\ell_{\sigma rb}$ the rotor bar leakage inductance, $\ell_{\sigma er}$ the rotor end ring segment leakage inductance, ℓ_{rr} the magnetizing inductance of rotor loop, and ℓ_{mr} the mutual inductance between two rotor loops.

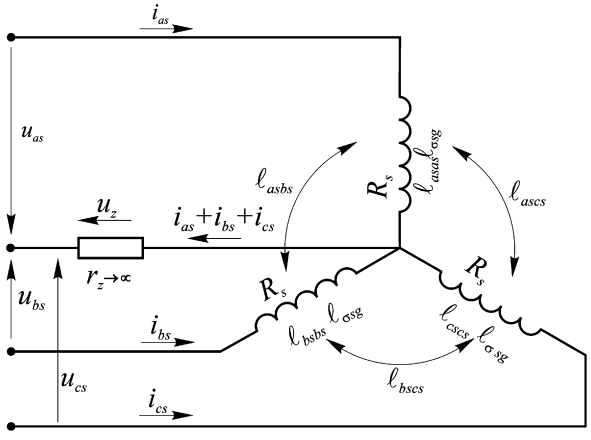

Fig. 1. Schematic representation of the stator windings.

Please cite this article as: G. Petrovic, et al., Sensorless speed detection of squirrel-cage induction machines using stator neutral point voltage..., Mechanical Systems and Signal Processing (2008), doi:10.1016/j.ymssp.2008.06.005

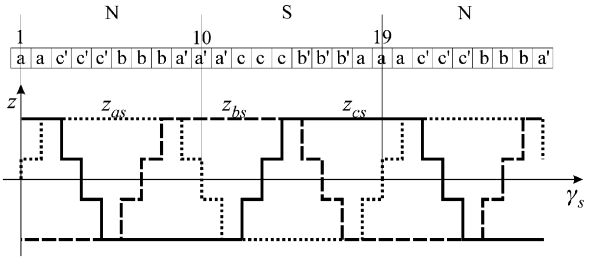

Fig. 2. Coil functions of the stator phases.

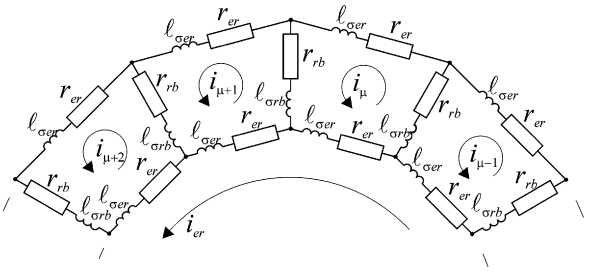

Fig. 3. Schematic representation of the rotor cage.

The rotor voltage equation in the matrix form can be written as

$$0 = \boldsymbol{R}_r \boldsymbol{i}_r + \frac{d\boldsymbol{\psi}_r}{dt}, \quad \boldsymbol{\Psi}_r = \boldsymbol{L}_{rs}\boldsymbol{i}_s + \boldsymbol{L}_r \boldsymbol{i}_r \tag{4}$$

The order of rotor submatrices and subvectors is equal to the number of rotor bars plus by one because of the rotor ring.

At the calculation of mutual inductance between the stator phase and the rotor loop $\ell_{as\mu}$, the rotor coil function $z(\vartheta,\gamma_s)$ depends on the angular position of the rotor (ϑ). Hence, Eq. (3) becomes

$$\ell_{as\mu}(\vartheta) = \frac{\mu_0}{\delta}\frac{d}{2} l_e \int_0^{2\pi} z_{as}(\gamma_s)\, z_{\mu}(\vartheta,\gamma_s)\, d(\gamma_s) \tag{5}$$

The end ring loop current does not couple with the stator windings. Therefore, the submatrix of mutual inductance between the stator and rotor becomes

$$\boldsymbol{L}_{sr}(\vartheta) = \begin{bmatrix} \ell_{as1}(\vartheta) & \ell_{as2}(\vartheta) & \dots & \ell_{asQr}(\vartheta) & 0 \\ \ell_{bs1}(\vartheta) & \ell_{bs2}(\vartheta) & \dots & \ell_{bsQr}(\vartheta) & 0 \\ \ell_{cs1}(\vartheta) & \ell_{cs2}(\vartheta) & \dots & \ell_{csQr}(\vartheta) & 0 \end{bmatrix} \tag{6}$$

Rotor bars skewing is taken into account in such a way that the length of the machine is divided in segments in the axial direction, for which rotor bars skewing is neglected. In that case, each segment is on a different magnetic position (ϑ+ϑ'). The segment of the rotor bar or the corresponding rotor loop, infinitesimal length dl, which is on place l measured from the center of machine in the axial direction, is shifted for angle ϑ' in the radial direction, and is calculated from the equation

$$\vartheta' = \frac{2\pi m_{sk}/Q_r}{l_e}\frac{2l}{d} \tag{7}$$

where m_{sk} is the skewing of rotor bars. A mutual inductance of the shifted segment $\ell'_{as\mu}$ per length unit is

$$\ell'_{as\mu}(\vartheta,\vartheta') = \frac{\mu_0}{\delta}\frac{d}{2}\int_0^{2\pi} z_{as}(\gamma_s) z_{\mu}(\vartheta+\vartheta',\gamma_s) d(\gamma_s) \tag{8}$$

After integrating along the axial direction, mutual inductance with skewing effect become [5]

$$\ell_{as\mu}(\vartheta) = \int_{-l_e/2}^{l_e/2} \ell'_{as\mu}\left(\vartheta, \frac{4\pi m_{sk} l}{Q_r l_e d}\right) dl \tag{9}$$

Please cite this article as: G. Petrovic, et al., Sensorless speed detection of squirrel-cage induction machines using stator neutral point voltage..., Mechanical Systems and Signal Processing (2008), doi:10.1016/j.ymssp.2008.06.005

For a complete mathematical description of the induction machine besides voltage equations, it is necessary to define a mechanical equation of motion as

$$\frac{d\omega}{dt} = \frac{1}{2H}(T_e - T_L), \quad \frac{d\vartheta}{dt} = \omega \tag{10}$$

where ω is the angular speed, ϑ the angular position of the rotor, H the rotor inertia, T_L the load torque, and T_e the electromagnetic torque, which is calculated from

$$T_e = (\boldsymbol{i}_s)^T \frac{d\boldsymbol{L}_{sr}}{d\vartheta} \boldsymbol{i}_r \tag{11}$$

3. Speed-detection algorithm

The neutral point voltage consists of information on machine speed. A relationship between induction machine speed and the frequency spectrum of neutral point voltage results from the geometry of the machine. Speed-related harmonics arise from variations in the air-gap permeance P_{ag} interacting with air-gap magnetomotive force, which produces an air-gap flux density [1,3]

$$B_{ag}(\gamma_s, \vartheta) = MMF_{ag}(\gamma_s, \vartheta) \cdot P_{ag}(\gamma_s, \vartheta) \tag{12}$$

where γ_s is the stator angular position, ϑ the mechanical rotor position, and MMF_{ag} the air-gap magnetomotive force resulting from the stator and rotor currents. The induced voltage in the stator coil is obtained from this flux density distribution. The sum of these phase voltages is the neutral point voltage. From fundamental principles, it can be shown [2,4] that these effects result in stator coils frequencies, and thus in neutral point voltage frequencies, described by

$$f_{sh} = f_1\left[(kQ_r + n_d)\left(\frac{1-s}{p}\right) + n_w\right] \tag{13}$$

where $k = 0, 1, 2, \ldots, Q_r$ is the number of rotor slots, $n_d = 0, \pm1, \pm2, \ldots$ the order of rotor eccentricity, s the per unit slip, p the number of pairs of poles and $n_w = \pm1, \pm3, \ldots$ the air-gap *MMF* harmonic order and f_1 is supply frequency.

In order to relate a particular slot harmonic frequency to the slip from Eq. (13), it is necessary to know n_d, n_w, and Q_r, which depend on the structural characteristics of the machine. As we examine slot harmonics, we can assume ideally centered rotor and therefore consider $n_d = 0$. The strongest harmonic is the first air-gap *MMF* harmonic and we can consider $n_w = \pm1$. Substituting $n_d = 0$ and $n_w = \pm1$ in Eq. (13), the frequency of the primary harmonic is obtained as

$$f_{\text{ecc}} = f_1\left[\frac{kQ_r}{p}(1-s) \pm 1\right] \tag{14}$$

Generally, the pair of harmonics is consistently the strongest, but in neutral point voltage only one of them appears. Therefore this harmonic is selected as primary slot harmonics and used for rotor speed detection. It is important to mention that neutral point voltage exists only if Q_r is a natural number except for a multiple of three [3]. From this harmonic, rotor speed is

$$n = \frac{60}{Q_r}(f_{\text{ecc}} - f_1) \tag{15}$$

In order to determine the slot harmonic frequency, the motor must be in the steady state so that f_1 and s are nearly constant; thus this technique works for any motor application that operates principally in the steady state.

Discrete Fourier Transform (DFT) was applied on a measured neutral point voltage to extract the spectral line:

$$U_z(k\,\Delta f) = \frac{1}{N}\sum_{n=0}^{N-1} w(nT)u_z(nT)e^{-j2\pi k\,\Delta f nT} \tag{16}$$

where $u_z(nT)$ are the samples of neutral point voltage, $w(nT)$ the window function, and N the number of samples. However, the DFT algorithm is limited by uncertainty principle states, which state that the frequency resolution (Δf) is fixed as the inverse of the sample length (NT). According to Eqs. (13) and (14), better speed determination accuracy is achieved by better frequency resolution obtained by the DFT procedure, which requires longer sample length. On the other hand, longer sample length increases the speed-detection error during dynamic conditions when the speed is changed. Reduction of sample length and at the same time keeping up frequency resolution can be obtained introducing adequate Hanning weighting function and interpolation spectrum algorithm.

The Hanning weighting function allows very accurate evaluations of the parameters characterizing each sinusoidal component of the signal, with a little increase in the computation time. It has been chosen because of its simple interpolation formula. If the k_rth spectral line returned by FFT operation on the windowed signal is a line of relative maximum in the spectrum $\overline{U}_z(k_r\,\Delta f)$, the "true" frequency f_{ecc} of the considered component can be expressed as [9]

$$f_{\text{ecc}} = (k_r + \partial_r)\Delta f \tag{17}$$

Please cite this article as: G. Petrovic, et al., Sensorless speed detection of squirrel-cage induction machines using stator neutral point voltage..., Mechanical Systems and Signal Processing (2008), doi:10.1016/j.ymssp.2008.06.005

where ∂_r is frequency displacement, and for the Hanning weighting function is

$$\partial_r = \frac{3}{2}\frac{\overline{U}_z(k_r)[\overline{U}_z(k_r+1)-\overline{U}_z(k_r-1)]}{[\overline{U}_z(k_r)+\overline{U}_z(k_r+1)][\overline{U}_z(k_r)+\overline{U}_z(k_r-1)]} \tag{18}$$

The only limitation in this procedure is that the minimum difference between two frequency components of the measured signal is greater than Δf.

4. Simulation results

For theoretical verification of the proposed speed-detection method, the simulation study is used prior to the laboratory test. The equation system (20) that presents the mathematical model of the squirrel-cage induction machine is solved using MATLAB simulation software. In order to obtain the stable simulation procedure, special care was paid to choice of resistance r_z value (Fig. 1). On the one hand, because of the modeling stator circuit without a neutral line, a sufficiently big value of the resistance r_z must be chosen. On the other hand, that resistance may not be too big because of the numerical stability problems. To solve this, the value of r_z is chosen to be 10^6 times bigger than the stator resistance. The ratings, parameters and windings specification of the induction machine used in the simulation and experimental study are given in Appendix A.

The neutral point voltage signal (u_z) and rotor speed, obtained by simulation, is used for the theoretical verification of the speed-detection algorithm described in the previous chapter. The sampling rate in all theoretical and experimental investigation is 50 kHz. All simulations were carried out with symmetrical three phase voltages. The accuracy of speed determination corresponds to the accuracy of the frequency determination of neutral point voltage primary harmonic. This accuracy depends on the time interval of sample length. For steady-state operation ($n = 1442$ rpm), the calculated primary harmonic frequency (f_{ecc}) of neutral point voltage as a function of sample length (NT) is shown in Fig. 4. As is expected, the better accuracy is obtained with longer sample length.

One can see that the primary harmonic frequency of neutral point voltage that corresponds to a rotor speed of 1442 rpm is 723 Hz and it can be determined with an accuracy of ± 0.25 Hz (± 0.5 rpm) for the sample length of 20 ms. By means of the FFT algorithm with window function, the calculated frequency, in the time domain, is in the middle of the data block. It means that calculated frequency has time delay for half of the data block. For the sample length of 20 ms, time delay of the calculated speed was 10 ms.

It is obvious that a bigger sample length increases the accuracy of speed detection at steady-state operation; however, on the other hand, at transient conditions a bigger sample length decreases that accuracy because of longer time delay. Therefore it is necessary to select the compromise sample length, which makes possible a satisfactory accuracy of speed detection at both steady-state and transient conditions.

The accuracy of speed determination at transient conditions is investigated by simulation of step change in load torque from nominal value to zero. The speed obtained by simulation using the induction machine mathematical model (n) and the speed calculated by means of the speed-detection algorithm (n') are shown in Fig. 5(a). Difference between these

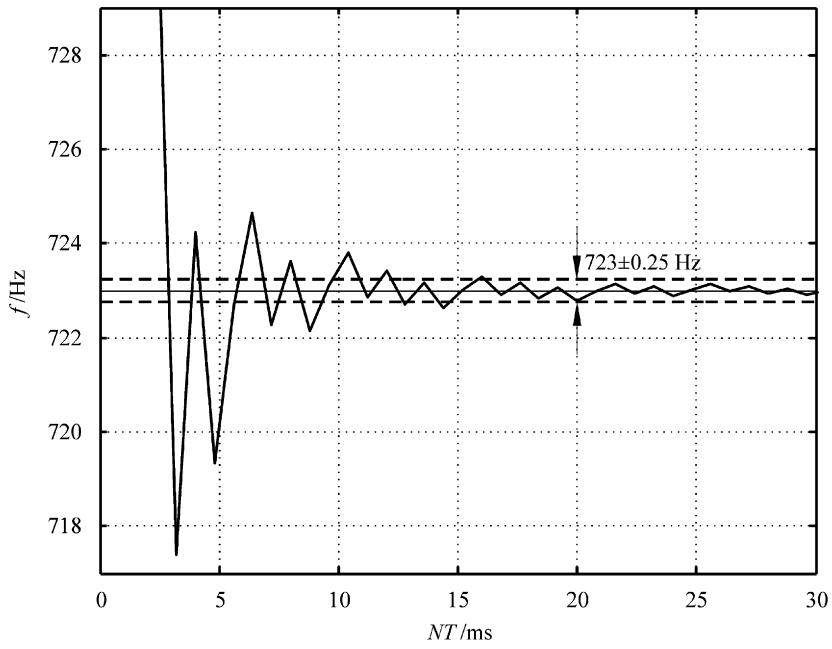

Fig. 4. Accuracy of the calculated primary harmonic frequency of neutral point voltage as a function of sample length.

Please cite this article as: G. Petrovic, et al., Sensorless speed detection of squirrel-cage induction machines using stator neutral point voltage..., Mechanical Systems and Signal Processing (2008), doi:10.1016/j.ymssp.2008.06.005

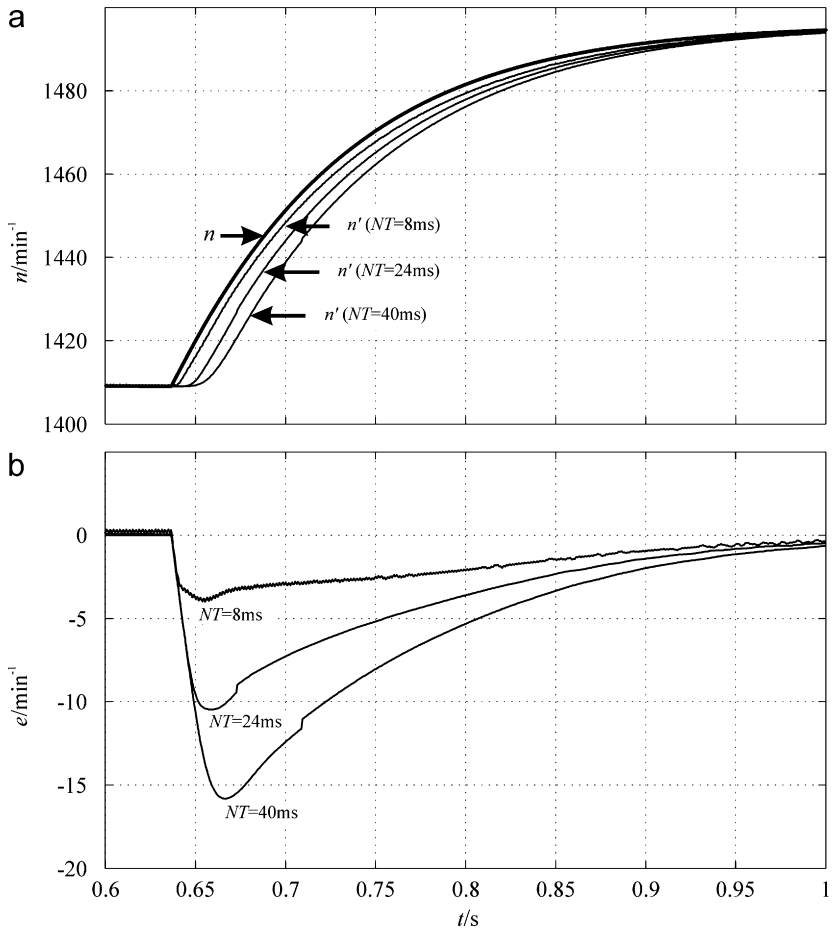

Fig. 5. The accuracy of the speed-detection algorithm in transient conditions for various sample lengths: (a) simulated (n) and calculated (n') rotor speed, (b) speed-detection error.

speeds is the error of the speed-detection algorithm (e) and it is shown in Fig. 5(b). The calculation of speed n' is performed for three sample lengths (NT). As is expected, for a longer sample length and faster change of the rotor speed, the error of the calculated speed is increased because of longer time delay.

5. Experimental results

The experimental verification of the speed-detection method based on neutral point voltage harmonics was performed using a 4-pole 2.2 kW induction motor with ratings and windings specifications given in Appendix A. Fig. 6 shows the experimental setup and block diagram of the speed-detection algorithm. The induction motor was loaded with a DC machine fed by a four-quadrant AC/DC converter. The speed-detection algorithm was implemented on a PC computer.

Fig. 7 shows the measured frequency spectrum of rotor slot harmonics under steady-state operation. The primary harmonic frequency is 730.4 Hz and using Eq. (15) the calculated rotor speed is 1458 rpm. Comparing this speed with the measured value obtained by means of an optical shaft encoder, a very good matching is shown, i.e. the error is less than 1 rpm.

Similarly as in simulation study, accuracy of the proposed method depending on the sample length was experimentally investigated (Fig. 8). In order to obtain the equal speed determination accuracy in steady-state operation by simulation results ($\pm$0.5 rpm), the time interval of the sample length needs to be 120 ms, which is 6 times greater than the one in simulation. According to the algorithm for the determination of rotor slot harmonic frequency (17) and (18), overlap of the neighboring harmonic reduces the accuracy of determination of frequency f_{ecc} and the motor speed. The greater errors by a smaller sample length appear only because of the 15th harmonic, which exists around the rotor slot harmonic of the neutral point voltage signal, as shown in Fig. 7. This harmonic originates from power supply and appears in the neutral point voltage signal because of the non-ideally balanced resistor star and it can be significantly reduced by improving simmetry of the resistor star.

Fig. 9 shows the actual (measured) and calculated rotor speed during a steady-state and transient operation in which the motor speed is changed approximately linearly from 1399 to 1494 rpm. The calculated rotor speed tracks the measured speed even during transients.

Please cite this article as: G. Petrovic, et al., Sensorless speed detection of squirrel-cage induction machines using stator neutral point voltage..., Mechanical Systems and Signal Processing (2008), doi:10.1016/j.ymssp.2008.06.005

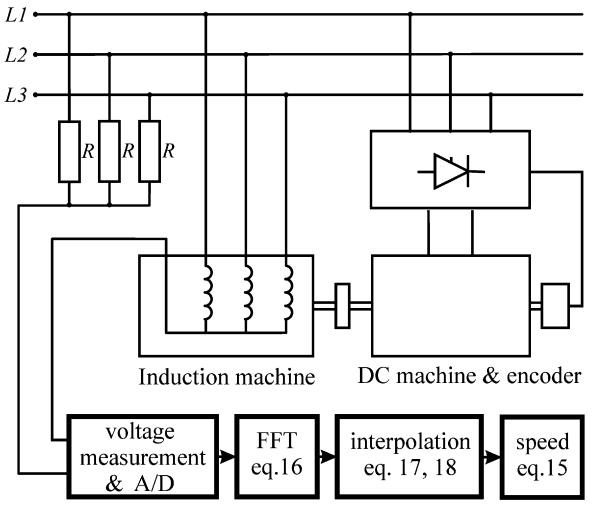

Fig. 6. Block diagram of the speed-detection method on the base of neutral point voltage harmonics.

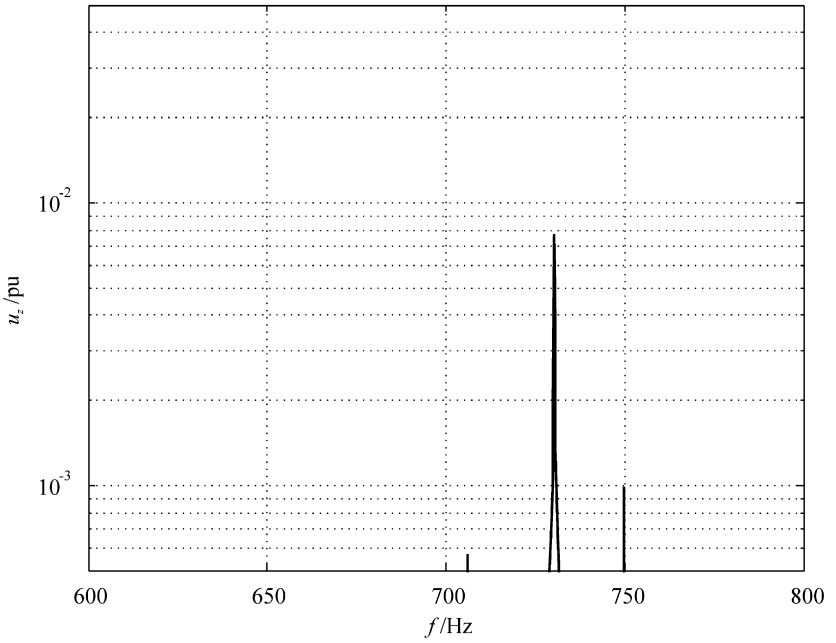

Fig. 7. Measured spectrum of rotor slot harmonics under steady-state operation at a speed of 1458 rpm.

As the speed is calculated using a sample length of 100 ms, the time delay of the calculated speed to the actual speed should be expected to be ~50 ms. But this time delay cannot be verified experimentally because the measured speed has also a time delay to the actual speed due to the process time of the encoder signal.

6. Conclusion

Experimental results have demonstrated that the proposed method reliably determines the rotor speed from neutral point voltage harmonics. The strongest harmonic in the stator windings neutral point voltage is the primary slot harmonic that we measure, while at the methods based on line current harmonic estimation, the primary slot harmonic is few orders lower than the fundamental current harmonic. Because of that, the current harmonic estimation methods need one more band pass filter. The main advantage of this method compared to the method based on current harmonics measuring is better accuracy and faster response.

Moreover, this technique is easy to implement and uses only low-cost instruments such as a commercial data acquisition board with low resolution. Better accuracy would be achieved for induction cage motors with a major number

Please cite this article as: G. Petrovic, et al., Sensorless speed detection of squirrel-cage induction machines using stator neutral point voltage..., Mechanical Systems and Signal Processing (2008), doi:10.1016/j.ymssp.2008.06.005

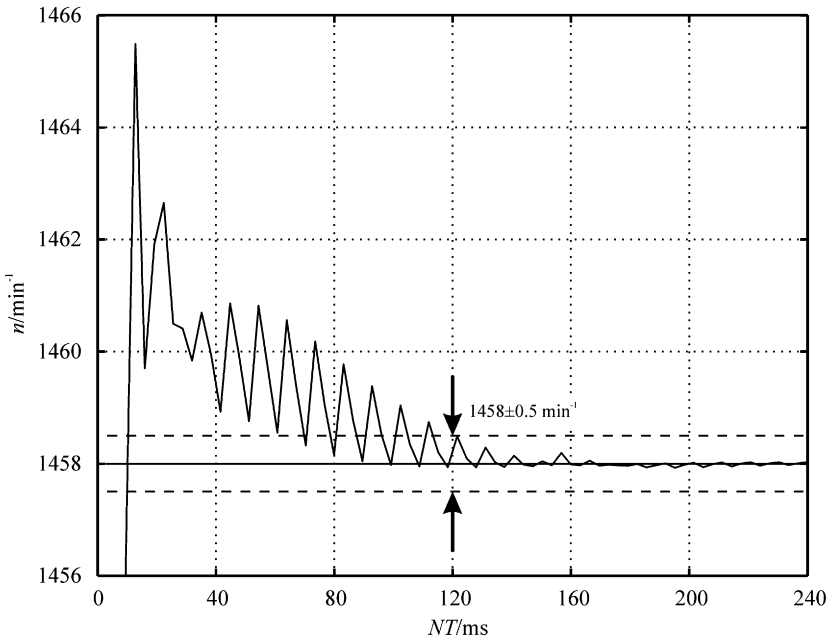

Fig. 8. Experimental results of the calculated speed at steady-state operation as a function of sample length.

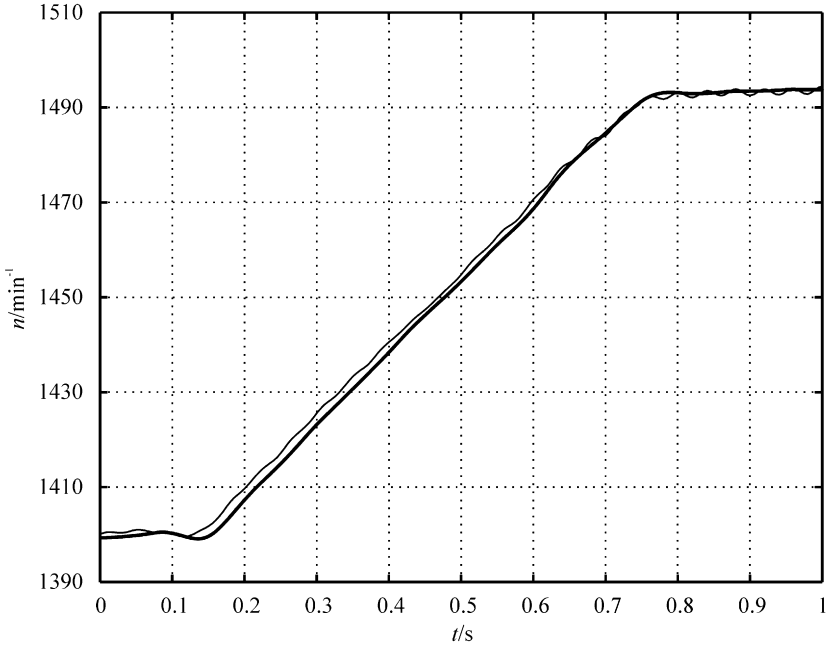

Fig. 9. Measured and calculated rotor speed during steady-state and transient conditions.

of rotor bars. This speed-detection method can enhance the performance and reliability of low- and medium-performance induction cage motor drives without a speed sensor.

Appendix A

Induction machine ratings are: 2.2 kW; 400 V; 50 Hz; 5.3 A; 1400 rpm.
Design machine parameters are given in Table 1, and the machine model parameters are given in Table 2.

Please cite this article as: G. Petrovic, et al., Sensorless speed detection of squirrel-cage induction machines using stator neutral point voltage..., Mechanical Systems and Signal Processing (2008), doi:10.1016/j.ymssp.2008.06.005

Table 1
Design machine parameters

Average air-gap radius	$d = 0.0895\,\text{m}$
Length of stator stack	$l_e = 0.090\,\text{m}$
Number of stator slots	$Q_s = 36$
Number of rotor bars	$Q_r = 28$
Turns per phase	$N_s = 246$
Turns per coil	$N_c = 41$
Number of poles	$2p = 4$
Skewing of rotor bars	$m_{sk} = 1.014$

Table 2
Machine model parameters

Parameter	(pu)
X_m main reactance	2.1782
r_s per-phase resistance	7.7273×10^{-2}
r_{er} rotor end ring segment resistance	5.1173×10^{-8}
r_{rb} rotor bar resistance	2.7131×10^{-6}
$l_{\sigma s}$ per phase leakage inductance	7.4562×10^{-2}
l_{asas} main inductance of the stator phase	1.5606
l_{asbs} mutual inductance between stator phases	6.4824×10^{-1}
l_{rr} main inductance of the rotor loop	1.7707×10^{-5}
l_{mr} mutual inductance between the two rotor loops	6.5583×10^{-7}
$l_{\sigma rb}$ rotor bar leakage inductance	9.1499×10^{-7}
$l_{\sigma er}$ rotor end-ring segment leakage inductance	7.8794×10^{-9}
max ($l_{as\mu r}$) maximum of mutual inductance between the stator phase and the rotor loop	1.1293×10^{-3}
H rotor inertia	8.5456

References

[1] K.D. Hurst, T.G. Habetler, Sensorless speed measurement using current harmonic spectral estimation in induction machine drives, IEEE Transactions on Power Electronics 11 (1) (1996) 66–73.
[2] K.D. Hurst, T.G. Habetler, A comparison of spectrum estimation techniques for sensorless speed detection in induction machines, IEEE Transactions on Industry Applications 33 (4) (1997) 898–905.
[3] M. Ishida, K. Iwata, A new slip frequency detector of an induction motor utilizing rotor slot harmonics, IEEE Transactions on Industry Applications IA-20 (1984) 575–582.
[4] M.E.H. Benbuozid, M. Vieira, C. Theys, Induction motors faults detection and localization using stator current advanced signal processing techniques, IEEE Transactions on Power Electronics 14 (1999) 14–22.
[5] G. Petrovic, Fault diagnosis of squirrel cage induction motor analysing line neutral voltage, Disertation, FESB Split, Croatia, 2006.
[6] V. Devanneaux, B. Dagues, J. Faucher, G. Barakat, An accurate model of squirrel cage induction machines under stator faults, Mathematics and Computers in Simulation, vol. 63, Elsevier, Amsterdam, 2003, pp. 377–391.
[7] H.A. Toliyat, T.A. Lipo, Transient analysis of cage induction machines under stator, rotor bar and end ring faults, IEEE Transactions on Energy Conversion 10 (2) (1995) 241–247.
[8] A. Ferrah, K.J. Bradley, P.J. Hogben-Laing, A speed identifier for induction motor drives using real-time adaptive digital filtering, IEEE Transactions on Industry Applications 34 (1) (1998) 156–162.
[9] G. Andria, M. Savino, A. Trotta, Windows and interpolation algorithms to improve electrical measurement accuracy, IEEE Transactions on Instrumentation and Measurement 38 (4) (1989) 856–863.

Please cite this article as: G. Petrovic, et al., Sensorless speed detection of squirrel-cage induction machines using stator neutral point voltage..., Mechanical Systems and Signal Processing (2008), doi:10.1016/j.ymssp.2008.06.005